Eur. Phys. J. A (2022) 58:212
https://doi.org/10.1140/epja/s10050-022-00869-6

THE EUROPEAN PHYSICAL JOURNAL A

Regular Article - Theoretical Physics

Probing nuclear observables via primordial nucleosynthesis

Ulf-G. Meißner[1,2,3,a], **Bernard Ch. Metsch**[4,5]

[1] Helmholtz-Institut für Strahlen- und Kernphysik and Bethe Center for Theoretical Physics, Rheinische Friedrich-Wilhelms Universität Bonn, 53115 Bonn, Germany
[2] Institute for Advanced Simulation (IAS-4), Institut für Kernphysik (IKP-3), Jülich Center for Hadron Physics, Forschungszentrum Jülich, 52425 Jülich, Germany
[3] Tbilisi State University, 0186 Tbilisi, Georgia
[4] Institute for Advanced Simulation (IAS-4), Forschungszentrum Jülich, 52425 Jülich, Germany
[5] Helmholtz-Institut für Strahlen- und Kernphysik, Rheinische Friedrich-Wilhelms Universität Bonn, 53115 Bonn, Germany

Received: 31 August 2022 / Accepted: 26 October 2022 / Published online: 8 November 2022

Communicated by Jérôme Margueron

Abstract We study the dependence of primordial nuclear abundances on fundamental nuclear observables such as binding energies, scattering lengths, neutron lifetime, etc. by varying these quantities. The numerical computations were performed with four publicly available codes, thus facilitating an investigation of the model-dependent (systematic) uncertainties on these dependences. Indeed deviations of the order of a few percent are found. Moreover, accounting for the temperature dependence of the sensitivity of the rates to some relevant parameters leads to a reduction of the sensitivity of the final primordial abundances, which in some cases is appreciable. These effects are considered to be relevant for studies of the dependence of the nuclear abundances on fundamental parameters such as quark masses or couplings underlying the nuclear parameters studied here.

1 Introduction

Primordial or Big Bang nucleosynthesis (BBN) is a fine laboratory to test our understanding of nuclear and particle physics, for some reviews see Refs. [1–4]. The light elements generated in BBN can nowadays be calculated from first principles, which offers the possibility to study in a model-independent way the dependence of the element abundances as a function of the fundamental parameters of the Standard Model of particle physics, in particular the light quark masses m_u, m_d and the QCD θ-parameter as well as the electromagnetic fine-structure constant α. This is based on the observation that the strong and the electromagnetic interactions both contribute to the nuclear binding, while the weak interactions makes their presence feel via certain decays, most prominently in the neutron decay into a proton and a lepton pair. In the Standard Model, the quark masses are given in terms of a priori unknown Yukawa couplings to the Higgs boson and the strength (coupling constants) of the various interactions must also be pinned down from experiment. It is therefore obvious that the Standard Model should be an effective field theory, which can eventually be derived from a more fundamental theory, such as string theory or alike. Another possibility is the Multiverse, in which our Universe is simply one particular manifestation with the Yukawa couplings and interaction strengths given as they are measured. Further, anthropic considerations come into play by asking how much these parameters can be modified to still allow for life on Earth (as given by the relative abundances of certain elements like ^{4}He, ^{12}C and ^{16}O without going into details of galaxy and planet formation and alike). For reviews on these issues, see e.g. Refs. [5–10].

Here, we wish to revisit recent works that have derived bounds on the fundamental parameters from element generation in BBN, see e.g. Refs. [11–15]. To really draw conclusions like that the Higgs vacuum expectation value can only be varied by about 1% [13,14] when keeping the Yukawa couplings constant, requires a full control of the systematic uncertainties in the calculation of BBN nucleosynthesis within our Universe. This is exactly what will be done in the present manuscript which will serve as the basis for future studies of the allowed quark mass and fine-structure constant variations within these uncertainties. In particular, we study the dependence of the element abundances on the nuclear reaction rates and also the temperature dependence of the direct and radiative capture reactions in the BBN network, that is most often neglected. Furthermore, variations in the neutron lifetime, the singlet neutron-proton scattering length

[a] e-mail: meissner@hiskp.uni-bonn.de (corresponding author)

as well as the deuteron binding energy are considered, where the latter two enter the leading reaction $n + p \to d + \gamma$, which is particular transparent using the effective field theory calculation of Refs. [16,17]. Most importantly, we utilize four different publicly available codes for BBN [4,18–23] to address the systematic uncertainties related to the modeling of the BBN network. In particular these codes differ in the number of nuclei and reactions taken into account as well as in the specific parametrization of the nuclear rates entering the coupled rate equations for the BBN network. Moreover, in determining the sensitivity of primordial abundances on nuclear parameters, we account for a temperature dependence of the variation of some rates on specific nuclear parameters and found that this leads in general to a reduction of these sensitivities in comparison to previous studies, where this temperature dependence was ignored. To our knowledge, such a comparative study has been not been published, but of course, new cosmological results are always used to update BBN, see e.g. Ref. [24].

The manuscript is organized as follows: In Sect. 2 we collect the basic formalism underlying BBN, which is required in what follows. In this section we also elaborate on the (pionless) Effective Field Theory description of the leading $n + p \to d + \gamma$ reaction. The BBN response matrix is introduced in Sect. 3. The numerical results of this study are presented in Sect. 4 and discussed in Sect. 5.

2 Basic formalism

The basic quantities to be determined in BBN are the nuclear abundances Y_{n_i}, where n_i denotes some nucleus. As pointed out e.g. in Refs. [4,20,23], the evolution of nuclear abundances Y_{n_i} is given generically by

$$\dot{Y}_{n_1} = \sum_{\substack{n_2,\ldots,n_p \\ m_1,\ldots,m_q}} N_{i_1} \left(\Gamma_{m_1,\ldots,m_q \to n_1,\ldots n_p} \frac{Y_{m_1}^{N_{m_1}} \cdots Y_{m_q}^{N_{m_q}}}{N_{m_1}! \cdots N_{m_q}!} - \Gamma_{n_1,\ldots,n_p \to m_1,\ldots m_q} \frac{Y_{n_1}^{N_{n_1}} \cdots Y_{m_q}^{N_{n_p}}}{N_{n_1}! \cdots N_{n_p}!} \right), \tag{1}$$

where the dot denotes the time derivative in a comoving frame, N_a is the stochiometric coefficient of species a in the reaction and where e.g. for a two-particle reaction $a + b \to c + d$, $\Gamma_{ab\to cd} = n_B \gamma_{ab\to cd}$ is the reaction rate with n_B the baryon volume density. This can readily be generalised to reactions involving more (or less) particles, see [4]. These equations are coupled via corresponding energy densities to the standard Friedmann equation describing the cosmological expansion in the early universe, for details and basic assumptions, see also [4,20,23].

2.1 Nuclear reaction rates

The average reaction rate $\gamma_{ab\to cd} = N_A \langle \sigma_{ab\to cd}\, v \rangle$ for a two-particle reaction $a + b \to c + d$ is obtained by folding the cross section $\sigma_{ab\to cd}(E)$ with the Maxwell–Boltzmann velocity distribution in thermal equilibrium

$$\gamma_{ab\to cd}(T) = N_A \sqrt{\frac{8}{\pi \mu_{ab} (kT)^3}} \int_0^\infty \mathrm{d}E\, E\, \sigma_{ab\to cd}(E)\, \mathrm{e}^{-\frac{E}{kT}}, \tag{2}$$

conventionally multiplied by Avogadro's number N_A, where μ_{ij} is the reduced mass of the nuclide pair ij, E is the kinetic energy in the center-of-mass (CMS) system, T is the temperature and k the Boltzmann constant. Defining $y := E/(kT)$ this can be written in the form

$$\gamma_{ab\to cd}(T) = N_A \sqrt{\frac{8\,kT}{\pi\, \mu_{ab}}} \int_0^\infty \mathrm{d}y\, \sigma_{ab\to cd}\,(kT\, y)\; y\, \mathrm{e}^{-y}, \tag{3}$$

which is suited for numerical computation e.g. with a Gauss-Laguerre integrator.

With the detailed balance relation

$$\sigma_{cd\to ab}\left(E'\right) = \frac{g_a\, g_b}{g_c\, g_d} \frac{p^2}{p'^2}\, \sigma_{ab\to cd}(E), \tag{4}$$

where

$$E = \frac{p^2}{2\,\mu_{ab}}, \quad E' = \frac{p'^2}{2\,\mu_{cd}}, \tag{5}$$

are the kinetic energies in the entrance and exit channels, respectively, and g_i is the spin multiplicity of particle i. Energy conservation leads to,

$$\begin{aligned} m_a + m_b + E &= m_c + m_d + E' \quad \text{or} \\ E' = E + Q, &\quad \text{with} \quad Q = m_a + m_b - m_c - m_d\,, \end{aligned} \tag{6}$$

in terms of the Q-value for the forward reaction. The inverse reaction rate is related to the forward rate as

$$\gamma_{cd\to ab}(T) = \left(\frac{\mu_{ab}}{\mu_{cd}}\right)^{\frac{3}{2}} \frac{g_a\, g_b}{g_c\, g_d}\, \mathrm{e}^{-\frac{Q}{kT}}\, \gamma_{ab\to cd}(T). \tag{7}$$

2.2 Q-value dependence of the reaction rates

The rates for nuclear reactions of the kind

$$a + b \to c + d \tag{8}$$

depend on the Q-value of the reaction, which in turn depends on the nuclear binding energies.

2.2.1 Varying nuclear binding energies

Now, e.g. for a relative change in the binding energy of nucleus a : $B_a \mapsto B_a\,(1+\delta_a)$ the nuclear mass change is given by

$$\Delta m_a = m_a - \delta_a\, B_a$$

and thus the reduced mass occurring in the expressions above changes as

$$\begin{aligned}
\mu_{ab} \mapsto \frac{(m_a-\delta_a\,B_a)\,m_b}{m_a-\delta_a\,B_a+m_b} &= \frac{m_a\,m_b-\delta_a\,B_a\,m_b}{(m_a+m_b)\left(1-\frac{\delta_a\,B_a}{m_a+m_b}\right)}\\
&\approx \left(\mu_{ab}-\frac{\delta_a\,B_a\,m_b}{m_a+m_b}\right)\left(1+\frac{\delta_a\,B_a}{m_a+m_b}\right)\\
&\approx \mu_{ab}\left(1+\frac{\delta_a\,B_a}{m_a+m_b}-\frac{\delta_a\,B_a}{m_a}\right)\\
&= \mu_{ab}\left(1-\frac{\delta_a\,B_a\,m_b}{(m_a+m_b)\,m_a}\right)\\
&= \mu_{ab}\left(1-\mu_{ab}\,\frac{\delta_a\,B_a}{m_a^2}\right). \qquad (9)
\end{aligned}$$

Since we shall consider fractional changes in the binding energy $\delta_a \approx \mathcal{O}(10^{-3})$ and $B_a/m_a \approx \mathcal{O}(10^{-2}-10^{-3})$, the change in the reduced masses is very small, $\mathcal{O}(10^{-5}$–$10^{-6})$ and this change in the reduced masses will therefore be neglected.

Noting that, since the total number of protons and neutrons is conserved in this kind of reaction: $Z_a+Z_b = Z_c+Z_d$, $N_a+N_b=N_c+N_d$,

$$\begin{aligned}
Q &= m_a+m_b-m_c-m_d\\
&= Z_a\,m_p+N_a\,m_n-B_a+Z_b\,m_p+N_b\,m_n-B_b\\
&\quad -Z_c\,m_p-N_c\,m_n+B_c-Z_d\,m_p-N_d\,m_n+B_d\\
&= B_c+B_d-B_a-B_b, \qquad (10)
\end{aligned}$$

a change in the binding energy will only affect the Q value:

$$\Delta Q = -\delta_a\,B_a-\delta_b\,B_b+\delta_c\,B_c+\delta_d\,B_d, \qquad (11)$$

where δ_i is the fractional change in the binding energy B_i of nuclide i and this will be the major effect to be studied below. We also note that in case of three-particle final states we shall use the same formula, e.g. by taking $^4\mathrm{He}+{}^4\mathrm{He}$ as $^8\mathrm{Be}$ and $p+n$ as d etc.

Note that, apart from the reaction $n+p\to d+\gamma$, to be discussed in some detail in Sect. 2.2.5, we do not make any assumptions concerning the binding energy dependence of the cross section itself, although, as has been argued in [11], e.g. a B_d^{-1} dependence for reactions involving deuterons might be considered.

2.2.2 Direct reactions $a+b\to c+d$:

Since the cross section is proportional to the final channel momentum p' and the probability of two charged nuclear particles overcoming their electrostatic barriers is given by the so called Gamow-Sommerfeld-factor [25]

$$\mathrm{e}^{-\sqrt{\frac{E'_G}{E'}}}, \quad \text{where} \quad E'_G = 2\pi^2\,Z_c^2\,Z_d^2\,\alpha^2\,\mu_{cd}\,c^2 \qquad (12)$$

is the so called Gamow-energy for the exit channel, Z_i is the charge number of nuclide i and $\alpha\simeq 1/137$ is the electromagnetic fine-structure constant, the Q-value dependence is given by

$$\sigma(Q;E)_{ab\to cd} \propto \sqrt{Q+E}\,\mathrm{e}^{-\sqrt{\frac{E'_G}{Q+E}}}. \qquad (13)$$

One thus finds for a change in the Q-value

$$\widetilde{Q} = Q_0+\Delta Q \qquad (14)$$

with

$$\left(\frac{\partial\sigma}{\partial Q}\right)(Q_0;E) = \frac{1}{2}\,\sigma(Q_0;E)\left(1+\sqrt{\frac{E'_G}{Q+E}}\right)\frac{1}{Q+E} \qquad (15)$$

that

$$\begin{aligned}
\sigma_{ab\to cd}(\widetilde{Q};E) &\approx \sigma_{ab\to cd}(Q_0;E)+\left(\frac{\partial\sigma}{\partial Q}(Q_0;E)\right)\Delta Q\\
&= \sigma_{ab\to cd}(Q_o;E)\left(1+\frac{\Delta Q}{2\,(Q_0+E)}\left(1+\sqrt{\frac{E'_G}{Q_0+E}}\right)\right). \qquad (16)
\end{aligned}$$

Thus, in linear approximation we have

$$\begin{aligned}
\gamma_{ab\to cd}(\widetilde{Q};T) &\approx \gamma_{ab\to cd}(Q_0;T)\\
&\quad +\sqrt{\frac{8}{\pi\,\mu_{ab}\,(kT)^3}}\int_0^\infty \mathrm{d}E\,E\,\sigma(Q_0;E)\\
&\quad \left(\frac{\Delta Q}{2\,(Q_0+E)}+\frac{\Delta Q\sqrt{E'_G}}{2\,(Q_0+E)^{\frac{3}{2}}}\right)\mathrm{e}^{-\frac{E}{kT}}\\
&=: \gamma_{ab\to cd}(Q_0;T)+\Delta\gamma(T)_{ab\to cd} \qquad (17)
\end{aligned}$$

and the determination of the temperature dependent Q-value change requires a separate computation of an integral over the cross section or, equivalently, over the astrophysical S-factor defined as

$$S(E) := \sigma(E)\,E\,\mathrm{e}^{\sqrt{\frac{E_G}{E}}}. \qquad (18)$$

We shall use a numerical integration of Eq. (17) to determine the Q-dependence of the rates for a dozen leading reactions in the BBN network.

If, however, we assume that for the relevant energies in the integrand $E \ll Q_0$, which might be the case for low temperatures, then this simplifies to

$$\begin{aligned}\gamma_{ab\to cd}(\widetilde{Q};T) &\approx \gamma_{ab\to cd}(Q_0;T)\\ &\quad\left(1+\frac{\Delta Q}{2\,Q_0}\left(1+\sqrt{\frac{E'_G}{Q_0}}\right)\right)\\ &= \gamma_{ab\to cd}(Q_0;T)\left(1+\frac{1}{2}\,\delta_Q\left(1+\sqrt{\frac{E'_G}{Q_0}}\right)\right)\\ &=: \gamma_{ab\to cd}(Q_0;T)+\Delta\gamma_{0;ab\to cd},\end{aligned} \tag{19}$$

where $\delta_Q = \Delta Q/Q_0$ is the fractional change in the Q-value. Indeed, Eq. (19) is the approximation that has been used in previous studies, such as e.g. Refs. [11–14]. Note that with this approximation the Q-value change is temperature independent.

2.2.3 Radiative capture reactions: $a + b \to c + \gamma$:

Assuming that the radiation is dominated by electromagnetic dipole transitions,[1] we have

$$\sigma(Q;E)_{ab\to c\gamma} \propto E_\gamma^3 \approx (Q+E)^3. \tag{20}$$

Accordingly, for a change in the Q-value

$$\widetilde{Q} = Q_0 + \Delta Q \tag{21}$$

with

$$\left(\frac{\partial\sigma}{\partial Q}\right)(Q_0;E) = 3\,\frac{\sigma(Q_0;E)}{Q_0+E} \tag{22}$$

one finds that

$$\begin{aligned}\sigma_{ab\to c\gamma}(\widetilde{Q};E) &\approx \sigma_{ab\to c\gamma}(Q_0;E)+\left(\frac{\partial\sigma}{\partial Q}(Q_0;E)\right)\Delta Q\\ &= \sigma_{ab\to c\gamma}(Q_o;E)\left(1+3\,\frac{\Delta Q}{Q_0+E}\right)\end{aligned} \tag{23}$$

and thus the change in the rate

$$\begin{aligned}\gamma_{ab\to c\gamma}(\widetilde{Q};T) &\approx \gamma_{ab\to c\gamma}(Q_0;T)\\ &\quad+3\,\Delta Q\sqrt{\frac{2}{\pi\,\mu_{ab}\,c^2\,(kT)^3}}\\ &\quad\times\int_0^\infty \mathrm{d}E\;\sigma(Q_0;E)\frac{E}{Q_0+E}\mathrm{e}^{-\frac{E}{kT}}\\ &=: \gamma_{ab\to c\gamma}(Q_0;T)+\Delta\gamma(T)_{ab\to c\gamma},\end{aligned} \tag{24}$$

as for the direct reactions before is temperature dependent.

[1] Note, however, that this not always the case, exceptions with appreciable $E2$ (electric quadrupole) contributions are e.g. the reactions: $^2\mathrm{H}+{}^2\mathrm{H}\to{}^4\mathrm{He}+\gamma$, $^2\mathrm{H}+{}^4\mathrm{He}\to{}^6\mathrm{Li}+\gamma$ and $^4\mathrm{He}+{}^{12}\mathrm{O}\to{}^{16}\mathrm{O}+\gamma$. We nevertheless always assume dipole dominance.

If again, as in Refs. [11–14], we assume that for the relevant energies in the integrand $E \ll Q_0$ then this simplifies to

$$\begin{aligned}\gamma_{ab\to c\gamma}(\widetilde{Q};T) &= \gamma_{ab\to c\gamma}(Q_0;T)\left(1+\frac{3\,\Delta Q}{Q_0}\right)\\ &= \gamma_{ab\to cd}(Q_0;T)\,(1+3\,\delta_Q)\\ &=: \gamma_{ab\to c\gamma}(Q_0;T)+\Delta\gamma_{0;ab\to c\gamma},\end{aligned} \tag{25}$$

where $\delta_Q := \Delta_Q/Q_0$. In this case:

$$Q = m_a + m_b - m_c = B_c - B_a - B_b \tag{26}$$

and a fractional change in the binding energy: $B_i \mapsto (1+\delta_i\,B_i)$ will be assumed, as above, to affect the Q value only:

$$\Delta Q = -\delta_a\,B_a - \delta_b\,B_b + \delta_c\,B_c. \tag{27}$$

2.2.4 Weak decay rates $a \to b + e^\pm + \overset{(-)}{\nu}$

Neglecting the nuclear recoil of the daughter nucleus, we have from energy conservation

$$M_a = M_b + E_e + E_\nu \tag{28}$$

and the maximum $e^\pm$ energy is given by

$$E_e^{max} = M_a - M_b =: Q \tag{29}$$

where M_a, M_b are the nuclear parent and daughter masses. Accordingly, the maximal $e^\pm$ momentum is given by

$$p_e^{max} = \sqrt{Q^2 - m_e^2} = m_e\sqrt{q^2-1},\quad q := \frac{Q}{m_e}. \tag{30}$$

The weak decay rate then reads [26]:

$$\lambda = \frac{G^2}{2\pi^3}\,\frac{m_p\,c^2}{\hbar}|M_{if}|^2\,f(Z,q), \tag{31}$$

where G is the weak (Fermi) coupling constant, M_{if} the nuclear matrix element and (ignoring Coulomb corrections):

$$\begin{aligned}f(q) &:= f(Z,q)|_{Z=0}\\ &= \frac{1}{60}\left[\sqrt{q^2-1}\,(2\,q^4-9\,q^2-8)\right.\\ &\quad\left.+15\,q\,\log(q+\sqrt{q^2-1})\right].\end{aligned} \tag{32}$$

From this an expression for the fractional change in the rate due to a change in the Q-value,

$$\begin{aligned}&\frac{\partial\log(f(q))}{\partial q}\\ &= \frac{\sqrt{q^2-1}\,\left(10\,q^3-25\,q\right)+15\,\log\left(q+\sqrt{q^2-1}\right)}{\sqrt{q^2-1}\,\left(2\,q^4-9\,q^2-8\right)+15\,q\,\log\left(q+\sqrt{q^2-1}\right)}\end{aligned} \tag{33}$$

follows, i.e.

$$\frac{\partial \log(\lambda)}{\partial q} = \frac{1}{\lambda}\frac{\partial \lambda}{\partial q} = \frac{\partial \log\left(f(q)\right)}{\partial q}. \tag{34}$$

With $\widetilde{Q} = Q_0 + \Delta Q = Q_0\,(1+\delta_Q)$, $\lambda_0 := \lambda(Q_0)$ and $q_0 := Q_0/m_e$, we find

$$\begin{aligned}\widetilde{\lambda} &= \lambda(Q_0) + \Delta\lambda \approx \lambda(Q_0) + \frac{\partial \lambda}{\partial Q}(Q_0)\,\Delta Q \\ &= \lambda(Q_0) + \frac{\partial \lambda}{\partial q}\,q_0\,\delta_Q = \lambda(Q_0) + \lambda_0\,\frac{\partial \log(\lambda)}{\partial q}\,q_0\,\delta_Q \\ &= \lambda(Q_0)\left(1 + q_0\,\frac{\partial \log(f(q))}{\partial q}\,\delta_Q\right).\end{aligned} \tag{35}$$

2.2.5 The leading reaction $n + p \to d + \gamma$

The formulas given above are the basis for the calculation of the primordial abundance variations mainly due to the dependence on the Q-values of most reactions in the BBN-network.

For the leading reaction $n + p \to d + \gamma$ in this network it is possible to study more details, since for this reaction an accurate description for the relevant energies in the framework of the so-called pionless effective field theory [16,17] is available. According to that work, the cross section for the capture reaction $n + p \to d + \gamma$ is given by

$$\sigma_{np\to d\gamma}(E) = \frac{4\pi\,\alpha\,\left(\gamma^2 + p^2\right)^3}{\gamma^3\,M_N^4\,p}\left[|\widetilde{\chi}_{M1}|^2 + |\widetilde{\chi}_{E1}|^2\right] \tag{36}$$

with $\alpha = e^2/\hbar c$ the electromagnetic fine-structure constant and $E = p^2/M_N$ is the total kinetic energy in the CMS, with p the magnitude of the momentum of either the proton or the neutron, and $\gamma := \sqrt{B\,M_N}$ is the "binding momentum" of the deuteron ground state.[2] The (dimensionless) electric dipole contribution is given up to N^{3}LO by

$$\begin{aligned}|\widetilde{\chi}_{E1}|^2 = \frac{\gamma^4\,M_N^2\,p^2}{(\gamma^2+p^2)^4}\Bigg[&\underbrace{1 + \gamma\,\rho_d + (\gamma\,\rho_d)^2 + (\gamma\,\rho_d)^3}_{\approx \frac{1}{1-\gamma\,\rho_d}} \\ &+ \frac{\gamma\,M_N}{6\pi}\left(\frac{\gamma^2}{3} + p^2\right) \\ &\times\left({}^{\not\pi}C_2^{(^3P_0)} + 2\,{}^{\not\pi}C_2^{(^3P_1)} + \frac{20}{3}\,{}^{\not\pi}C_2^{(^3P_2)}\right)\Bigg],\end{aligned} \tag{37}$$

where ρ_d is the effective range. We use the numerical values from Ref. [16] , $\gamma^{-1} = 4.318\,946$ fm, $\rho_d = 1.764 \pm 0.002$ fm, ${}^{\not\pi}C_2^{(^3P_0)} = 6.53$ fm^4, ${}^{\not\pi}C_2^{(^3P_1)} = -5.91$ fm^4, ${}^{\not\pi}C_2^{(^3P_0)} = 0.57$ fm^4. Furthermore, the magnetic dipole contribution at NLO reads

$$\begin{aligned}|\widetilde{\chi}_{M1}|^2 = &\frac{\gamma^4\,\kappa_1^2\,(1-a_s\,\gamma)^2}{\left(1+a_s^2\,\gamma^2\right)\left(\gamma^2+p^2\right)^2} \\ &\times\Bigg[1 + \gamma\,\rho_d - \frac{r_0}{a_s}\,\frac{\left(\gamma\,a_s + a_s^2\,p^2\right)a_s^2\,p^2}{\left(1+a_s^2\,p^2\right)(1-a_s\,\gamma)} \\ &- \frac{{}^{\not\pi}L_{np}}{\kappa_1}\,\frac{a_s\,M_N}{2\pi}\,\frac{\gamma^2+p^2}{1-a_s\,\gamma}\Bigg],\end{aligned} \tag{38}$$

where $\kappa_1 = (\mu_p - \mu_n)/2$ is the nucleon isovector magnetic moment (in units of $\mu_N = e\,\hbar/(M_N\,c)$), a_s is the scattering length and r_0 is the effective range in the ${}^1S_0$-channel. Again we use the numerical values from Ref. [16] , $a_s = -23.714 \pm 0.013$ fm, $r_0 = 2.73 \pm 0.03$ fm, ${}^{\not\pi}L_{np} = -4.513$ fm^2. The resulting cross section is compared to experimental data in Fig. 1.

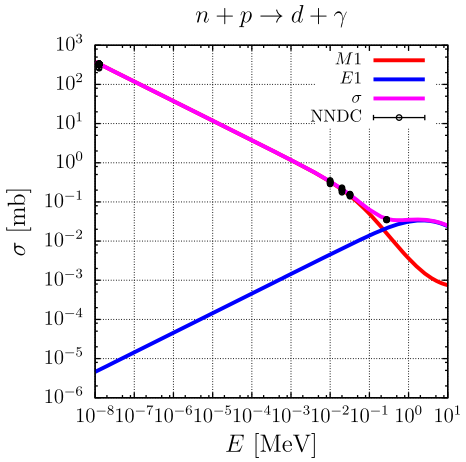

Fig. 1 Radiative capture $n + p \to d + \gamma$ cross section (in mb) (magenta, color online) as a function of the CMS kinetic energy in MeV, from [17]; the calculated $M1$ (red) and $E1$ (blue) contributions to the cross section are also shown separately. Experimental data later than 1960 are from NNDC online [27]

Considering only the leading contributions one finds

$$\sigma_{M1;np\to d\gamma}(p) = \frac{\pi\,\alpha\,\left(\mu_n - \mu_p\right)^2\,\gamma\,\left(\gamma^2+p^2\right)\,(1-a_s\,\gamma)^2}{M_N^4\,p\,\left(1+a_s^2\,p^2\right)}. \tag{39}$$

With $p = \sqrt{M_N\,E}$, $\gamma = \sqrt{M_N\,B_d}$ (B_d the binding energy of the deuteron) and introducing W via $a_s =: -1/\sqrt{M_N\,W}$ this reads

$$\begin{aligned}\sigma_{M1;np\to d\gamma}(E) = \pi\,&\frac{\alpha}{M_N^2}\,\left(\mu_n - \mu_p\right)^2 \\ &\times\frac{\sqrt{B_d}\,(B_d + E)\left(\sqrt{B_d} + \sqrt{W}\right)^2}{M_N\,\sqrt{E}\,(E+W)}.\end{aligned} \tag{40}$$

[2] Here it is understood that all energies are expressed through equivalent wave numbers, *i.e.* $p \mapsto p\,c/(\hbar c)$, $M \mapsto M\,c^2/(\hbar c)$, $\gamma \mapsto \sqrt{B\,M\,c^2}/(\hbar c)$, etc., all in units of fm^{-1}. The cross section is then given in units of fm^2 = 10 mb.

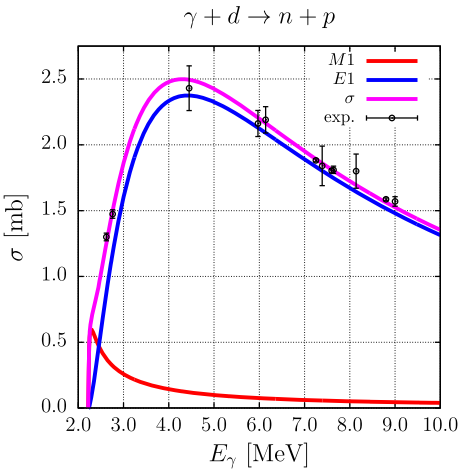

Fig. 2 Photodisintegration $\gamma + d \to n + p$ cross section (in mb) (magenta, color online) as a function of the (laboratory) photon energy in MeV, from [17]. The calculated $M1$ (red) and $E1$ (blue) contributions to the cross section are also shown separately. Experimental data from Ref. [28]

Likewise

$$\sigma_{E1;np\to d\gamma}(p) = \frac{4\pi\,\alpha\,p\,\gamma}{M_N^2\,\left(\gamma^2+p^2\right)\,(1-\gamma\,\rho_d)} \tag{41}$$

or, with $\rho_d =: 1/\left(\sqrt{M_N\,R}\right)$,

$$\sigma_{E1;np\to d\gamma}(E) = 4\pi\,\frac{\alpha}{M_N^2}\,\frac{\sqrt{E\,B_d}}{(E+B_d)\left(1-\sqrt{\frac{B_d}{R}}\right)}. \tag{42}$$

The cross section for the inverse reaction can be obtained via

$$\begin{aligned}\sigma_{\gamma\,d\to np}\left(E_\gamma\right) &= \frac{2}{3}\,\frac{p^2}{k^2}\,\sigma_{np\to d\gamma}\left(E_\gamma - B_d\right)\\ &= \frac{2}{3}\,\frac{M_N c^2\,\left(E_\gamma - B\right)_d}{E_\gamma^2}\,\sigma_{np\to d\gamma}\left(E_\gamma - B_d\right)\end{aligned} \tag{43}$$

with $E_\gamma = K$ the photon energy in the rest frame of the deuteron, where we used $k \approx K$ and

$$\begin{aligned}p^2 &\approx M_N\,(k-B_d) \approx M_N\,(K-B_d) = M_N\,k - \gamma^2\\ &\Leftrightarrow\quad p^2+\gamma^2 \approx M_N\,k \approx M_N\,K\end{aligned} \tag{44}$$

as well as the ratio of the statistical weights

$$\frac{g_p\,g_n}{g_\gamma\,g_d} = \frac{2\cdot 2}{2\cdot 3} = \frac{2}{3}. \tag{45}$$

and

$$E = \frac{p^2}{M_N} \approx k - B_d \approx K - B_d = E_\gamma - B_d. \tag{46}$$

We thus find for the photodisintegration reaction

$$\begin{aligned}&\sigma_{M1;\gamma d\to np}(p)\\ &= \frac{2\pi}{3}\,\alpha\,\frac{\left(\mu_n-\mu_p\right)^2\,p^2\,\gamma\,\left(\gamma^2+p^2\right)^2\,(1-a_s\,\gamma)^2}{k^2\,M_N^4\,p\,\left(\gamma^2+p^2\right)\left(1+a_s^2\,p^2\right)}\\ &= \frac{2\pi}{3}\,\frac{\alpha}{M_N^2}\,\left(\mu_n-\mu_p\right)^2\,\frac{p\,\gamma\,(1-a_s\,\gamma)^2}{\left(\gamma^2+p^2\right)\left(1+a_s^2\,p^2\right)}\\ &= \frac{2\pi}{3}\,\frac{\alpha}{M_N^2}\,\left(\mu_n-\mu_p\right)^2\,\frac{\sqrt{B_d}\,\sqrt{E_\gamma-B_d}\,\left(\sqrt{B_d}+\sqrt{W}\right)^2}{E_\gamma\,\left(E_\gamma-B_d+W\right)}\\ &= \sigma_{M1;\gamma d\to np}(E_\gamma),\end{aligned} \tag{47}$$

where we used $W = (M_N\,a_s^2)$. This indeed corresponds to the Bethe-Longmire zero range expression, see Eq. (56) of Ref. [29]. For the electric dipole contribution to the photodisintegration cross section one finds the zero-range expression

$$\begin{aligned}&\sigma_{E1;\gamma d\to np}(p)\\ &= \frac{8\pi}{3}\,\alpha\,\frac{p^3\,\gamma\,\left(\gamma^2+p^2\right)^2}{k^2\,M_N^2\,\left(\gamma^2+p^2\right)^3}\\ &= \frac{8\pi}{3}\,\alpha\,\frac{\gamma\,p^3}{\left(\gamma^2+p^2\right)^3} = \frac{8\pi}{3}\,\frac{\alpha}{\gamma^2}\,\frac{(p\,\gamma)^3}{\left(\gamma^2+p^2\right)^3}\\ &= \frac{8\pi}{3}\,\frac{\alpha}{\gamma^2}\,\frac{M_N^3\,B_d^3\,(1-\eta)^{\frac{3}{2}}}{M_N^3\,E_\gamma^3} = \frac{8\pi}{3}\,\frac{\alpha}{\gamma^2}\,\frac{(1-\eta)^{\frac{3}{2}}}{\eta^3}\\ &= \frac{8\pi}{3}\,\frac{\alpha}{M_N}\,\frac{\sqrt{B_d}\,\left(E_\gamma-B_d\right)^{\frac{3}{2}}}{E_\gamma^3}\\ &= \sigma_{E1;\gamma d\to np}(E_\gamma)\end{aligned} \tag{48}$$

where $\gamma^2 + p^2 \approx M_N\,k \approx M_N\,K =: M_N\,E_\gamma$ and $\eta := E_\gamma/B_d$, corresponding to the expression of Eq. (16) in [30], first derived by Bethe and Peierls. The effective range correction (see Eq. (6) in [29]) to this is given by the factor $(1-\gamma\,\rho_d)^{-1}$. The result from the N^{3}LO-calculation of [17] is compared to experimental data in Fig. 2.

Therefore, for this leading reaction in the BBN-network a sufficiently accurate description of the experimental data is available. Moreover, this EFT-description allows to study the variation of the cross section due to changes in nuclear parameters, such as the deuteron binding energy B_d, the $^1S_0$ np scattering length a_s, the corresponding effective range r_0 as well as the effective range ρ_d in the deuteron channel of np-scattering. Below we shall concentrate on the dependence on B_d and a_s, since these give the leading effects.

In Fig. 3 the numerically calculated rate according to Eq. (2) for the $n + p \to d + \gamma$ reaction is shown and compared to the parameterizations used in the original version of the codes. Apart from the original `NUC123` parametrisation, see [31], these curves are very consistent. In the rest of this paper, the parameterization according to a rational function fit of the form

$$f(t) = c_0,\ \frac{1+\sum_{i=1}^5 c_i\,t^i}{1+\sum_{i=1}^4 d_j\,t^j} \tag{49}$$

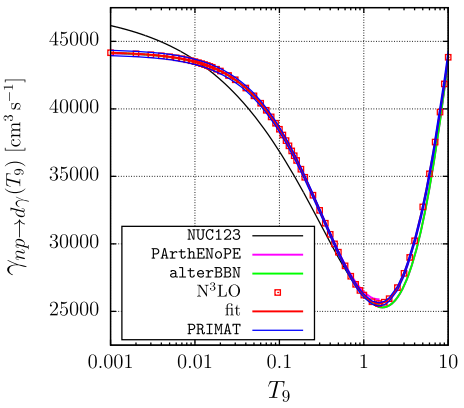

Fig. 3 The temperature dependent rate (in units of cm^3 s^{-1}) calculated from the cross section of the $n+p \to d+\gamma$ reaction in N^{3}LO and compared to the parameterizations used in the programmes `NUC123` [18] (in black, color online), `PArthENoPE` [23] (in magenta), `AlterBBN` [20] (in green) and `PRIMAT` [4] for which the two blue curves correspond to the lower and upper limit of the rate. The red solid curve represents a rational function fit to the red data points. $T_9 := T/[10^9\,\mathrm{K}]$

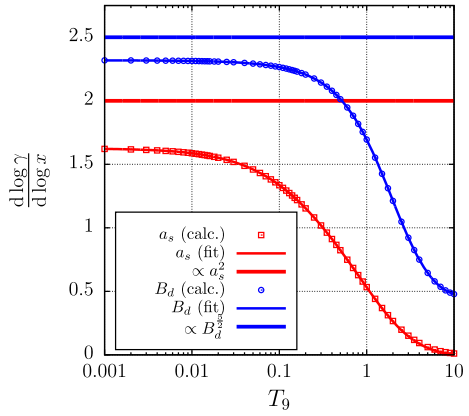

Fig. 4 Temperature dependence of the fractional change in the rate γ of the $n+p \to d+\gamma$ reaction, due to a fractional change in $x = a_s$ (in red, color online) or $x = B_d$ (in blue): $\frac{\partial \log\gamma}{\partial \log x}$. Data points are from a numerical evaluation of Eq. (2), the thin solid lines represent a rational function fit to these data and the thick solid lines represent the powers found in the extreme low energy (or low temperature) limit. $T_9 := T/[10^9\,\mathrm{K}]$

to the calculated rate based on the N^{3}LO-cross section is used throughout in all programmes.

From the formulas above in leading order, i.e. at very low energies, where the $M1$-contribution dominates, the dependence of the cross section and hence of the rate of the $n+p \to d+\gamma$ reaction is found to be

$$\gamma_{M1;np\to d\gamma} \propto B_d^{\frac{5}{2}}\, a_s^2, \tag{50}$$

leading to

$$\frac{\partial \log\gamma}{\partial \log a_s} = 2, \qquad \frac{\partial \log\gamma}{\partial \log B_d} = \frac{5}{2}, \tag{51}$$

which are energy or temperature independent. However, taking into account the full N^{3}LO-expressions above, this is found to vary appreciably in the BBN-relevant range $10^{-3} \le T_9 \le 10$, with $T_9 := T/[10^9\,\mathrm{K}]$, leading to a rather strong suppression of the dependence at high temperatures, see Fig. 4.

2.2.6 *Temperature dependence of the rates for the leading reactions*

Such a suppression, in particular for the dependence on the binding energies, is to be expected for the other nuclear reactions also. However, for most reactions the data for the rates are given in the form of parameterizations as a function of T_9 or in the form of tables. Only if the cross-sections $\sigma(E)$, or, equivalently, the astrophysical $S(E)$-function is available, it is possible to study the temperature dependence of a change in the rate γ due to a change in the binding energy or Q-value according to Eqs. (17, 24). To this end we numerically compute the integrals in these equations and then fit the ratio of the change in the rate $\Delta\gamma(T_9)/\Delta\gamma_0$ according to Eqs. (17, 19) for direct reactions or Eqs. (24,25) for radiative capture reactions by a rational function of the form

$$g(T_9) = \frac{1 + r_1\, T_9 + r_2\, T_9^2 + r_3\, T_9^3}{1 + q\, T_9}. \tag{52}$$

This is then used in the rate equations. We do this for the leading reactions in the BBN-network, viz. the radiative capture reactions

$$\begin{aligned} &p + {}^2\mathrm{H} \to {}^3\mathrm{He} + \gamma, \quad p + {}^3\mathrm{H} \to {}^4\mathrm{He} + \gamma, \\ &{}^3\mathrm{H} + {}^4\mathrm{He} \to {}^7\mathrm{Li} + \gamma, \quad {}^3\mathrm{He} + {}^4\mathrm{He} \to {}^7\mathrm{Be} + \gamma, \\ &{}^2\mathrm{H} + {}^4\mathrm{He} \to {}^6\mathrm{Li} + \gamma, \quad p + {}^7\mathrm{Li} \to {}^4\mathrm{He} + {}^4\mathrm{He} + \gamma, \end{aligned} \tag{53}$$

the charge exchange reactions

$$n + {}^3\mathrm{He} \to {}^3\mathrm{H} + p, \quad n + {}^7\mathrm{Be} \to {}^7\mathrm{Li} + p, \tag{54}$$

and the other direct reactions

$$\begin{aligned} &{}^2\mathrm{H} + {}^2\mathrm{H} \to {}^3\mathrm{H} + p, \quad {}^2\mathrm{H} + {}^2\mathrm{H} \to {}^3\mathrm{He} + n, \\ &{}^2\mathrm{H} + {}^3\mathrm{H} \to {}^4\mathrm{He} + n, \quad {}^2\mathrm{H} + {}^3\mathrm{He} \to {}^4\mathrm{He} + p, \\ &p + {}^7\mathrm{Li} \to {}^4\mathrm{He} + {}^4\mathrm{He}, \quad p + {}^6\mathrm{Li} \to {}^3\mathrm{He} + {}^4\mathrm{He}, \\ &{}^2\mathrm{H} + {}^7\mathrm{Be} \to {}^4\mathrm{He} + {}^4\mathrm{He} + p, \end{aligned} \tag{55}$$

for which parameterizations of the energy dependence of the cross section can e.g. be found in Appendix D of [32]. For some selected reactions the calculated ratios $\Delta\gamma(T_9)/\Delta\gamma_0$ together with the rational function fit are shown in Fig. 5, showing that for temperatures $T_9 > 0.1$ this change is indeed generally suppressed with respect to the change calculated with Eqs. (19, 25)

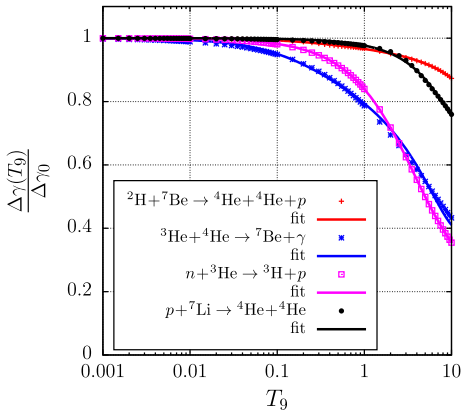

Fig. 5 Temperature dependence of the change in the rate $\Delta\gamma(T_9)/\Delta\gamma_0$ for a fractional change in the Q-value of some selected leading reactions, due to a fractional change in $x = a_s$ or $x = B_d$: $\frac{\partial \log\gamma}{\partial \log x}$. Data points are from a numerical evaluation of Eqs. (17, 24); solid lines (color online) represent the rational function fits used in subsequent calculations. $T_9 := T/[10^9\,\mathrm{K}]$

3 The BBN response matrix

We estimate the linear dependence of primordial abundances Y_n on small changes in the neutron life time τ_n, the nuclear binding energies B_a and the $^1S_0$ np scattering length a_s, $\partial \log Y_n/\partial \log X_k$, by calculating the abundance of the nuclide

$$n \in \left\{{}^2\mathrm{H}, {}^3\mathrm{H} + {}^3\mathrm{He}, {}^4\mathrm{He}, {}^6\mathrm{Li}, {}^7\mathrm{Li} + {}^7\mathrm{Be}, \right\} \tag{56}$$

i.e.

$$Y_n\left(X_k\,(1+\delta_k)\right), \qquad X_k \in \{\tau_n, B_a, a_s\} \tag{57}$$

for fractional changes $\delta_k \approx \mathcal{O}(10^{-3})$ in the nuclear parameters X_k with the publicly available codes for BBN: A version of the Kawano code called `NUC123` [18] (in `FORTRAN`), two more modern implementations based on this: `PArthENoPE` [21–23] (`in FORTRAN`) and `AlterBBN` [19,20] (in `C`) as well as an implementation as a `mathematica`-notebook: `PRIMAT` [4]. To this end we perform a least-squares fit of a quadratic polynomial to the abundances:

$$P_k(\delta_k) := c_0\left(1 + c_1\,\delta_k + c_2\,\delta_k^2\right), \tag{58}$$

such that

$$\frac{\partial}{\partial c_j}\left|Y_n\left(X_k\,(1+\delta_k)\right) - P_k(\delta_k)\right|^2 = 0, \quad j = 0, 1, 2. \tag{59}$$

Then

$$\frac{\partial \log Y_n}{\partial \log X_k} \approx c_1 \tag{60}$$

will be called an element of the (linear) nuclear BBN response matrix. It represents the (dimensionless) fractional change in the primordial abundance Y_n due to a fractional change in the nuclear parameter X_k in linear approximation. This method was preferred over a direct approximation of the (logarithmic) derivatives via finite differences, since some of the calculated abundances turned out to be rather noisy in particular when close to zero.

4 Numerical results

In what follows, we use $\eta = 6.14 \times 10^{-10}$ from [37] as the baryon-to-photon density ratio, but we will also allow for variations of this parameter. In all programmes, the following modifications were made:

- All natural constants were updated to recent values listed by CODATA [33] and PDG [36,37];
- Atomic mass excesses were taken from the NUBASE2020 [34] compilation; nuclear binding energies were then calculated by accounting for the atomic binding energies from [35], although this is a minor effect;
- Reverse reaction rate constants were recalculated on the basis of the nuclear data above;
- In `NUC123` hard coded constants were substituted by their analytical expressions in terms of natural constants updated from CODATA [33] and PDG [36,37].

In addition, and also in the `primat`-implementation [4], the rate of the $n + p \to d + \gamma$ radiative capture reaction was calculated on the basis of the analytical expression for the cross section from the EFT calculation in [17], see also Sect. 2 and rational function fits of the temperature dependence and the dependencies on the deuteron binding energy and the $^1S_0$ np scattering length, as explained in Sect. 3 were used.

For the fractional change in the rate due to changes in the Q-values of direct reactions we used the expression of Eqs. (19, 25) with the exception of the reactions listed in Eqs. (53, 54 and 55), where we used Eqs. (17, 24). For the Q-value dependence of the weak decay rates we used Eqs. (33, 35).

The values obtained with each of the programmes for the abundances at the end of the BBN-epoch in terms of the number ratios $Y_{^2\mathrm{H}}/Y_\mathrm{H}$, $Y_{^3\mathrm{H}+^3\mathrm{He}}/Y_\mathrm{H}$, $Y_{^6\mathrm{Li}}/Y_\mathrm{H}$, $Y_{^7\mathrm{Li}+^7\mathrm{Be}}/Y_\mathrm{H}$, and the mass ratio for ^{4}He are listed in Table 1. The discrepancy of about a factor of three in the abundance ratio of ^{7}Li + ^{7}Be to H is known as the "Li-problem", see [37] and references therein. Here various possible explanations of this discrepancy are discussed: e.g. systematic errors in the observed lithium-abundance and in the determination of the primordial abundance from these observations, possible issues in stellar astrophysics leading to the destruction of lithium and/or obscuring lithium from detection, uncertainties in nuclear reaction input data, fluctuations in the baryon-to-photon ratio, effects from decays of beyond-the-

Table 1 Final abundances as number ratios Y_n/Y_H (for ^{4}He the mass ratio Y_p) calculated with the modified versions of the codes

code	^{2}H $\times 10^5$	^{3}H $+^3$He $\times 10^5$	Y_p	^{6}Li $\times 10^{14}$	^{7}Li $+^7$Be $\times 10^{10}$
NUC123	2.550	1.040	0.247	1.101	4.577
parthenope	2.511	1.032	0.247	1.091	4.672
alterbbn	2.445	1.031	0.247	1.078	5.425
primat	2.471	1.044	0.247	1.198	5.413
PDG [37]	2.547		0.245		1.6
$\pm$	0.025		0.003		0.3

The nominal reaction Q_0-values used were calculated from the nuclear binding energies taken from [34], furthermore $\eta = 6.14 \times 10^{-10}$ and $\tau_n = 879.4$ s

standard-model particles leading to non-equilibrium nucleons dissociating light elements or changes in fundamental natural constants. In spite of this unresolved issue in BBN the consistency of the cosmic microwave background observations with the determined abundances of deuterium and helium is considered in [37] to be a "non-trivial success". Accordingly, we think that this issue is no obstacle for the study presented here.

In order to determine the sensitivity of the abundances, each of the programmes was run for fractional changes of the parameters τ_n, a_s, $B_{^2\mathrm{H}}$, $B_{^3\mathrm{H}}$, $B_{^3\mathrm{He}}$, $B_{^4\mathrm{He}}$, $B_{^6\mathrm{Li}}$, $B_{^7\mathrm{Li}}$ and $B_{^7\mathrm{Be}}$ for about a dozen equidistant values in a range $[-\delta, \delta]$, $\delta \approx \mathcal{O}(10^{-4}$–$10^{-3})$.

The elements of the response matrix were then determined by a polynomial fit, as explained above in Sect. 3 for the abundances of $Y_{^2\mathrm{H}}/Y_{\mathrm{H}}$, $Y_{^3\mathrm{H}+^3\mathrm{He}}/Y_{\mathrm{H}}$, $Y_{^6\mathrm{Li}}/Y_{\mathrm{H}}$, $Y_{^7\mathrm{Li}+^7\mathrm{Be}}/Y_{\mathrm{H}}$, and the mass ratio for ^{4}He.

The values for the resulting response matrix elements are given and compared to some results from the literature in Table 2.

In order to illustrate the dependence on the baryon-to-photon density parameter η we displayed in Fig. 6 the variation of the response matrix elements for a change of η in the range 5.94×10^{-10}–6.34×10^{-10} which corresponds to the error range quoted in [37]: $\eta_{10} := \eta \times 10^{10} = 6.143 \pm 0.190$.

The following observations can be made:

- Concerning the baryon-to-photon density ratio η-dependence : Although the final abundances at the end of the primordial nucleosynthesis do depend on η strong enough and, in particular the ^{4}He and deuteron abundances allow for estimating a rather strict bound on η, see e.g. Fig. 24.1 in section 24 of [37] compatible with the CMB determination of the cosmic baryon density [37], the η-dependence of the linear response to the nuclear parameters studied here was found to be in general almost linear and of rather moderate size, see Fig. 6. Note that a conspicuous correlation between the values for the response matrix elements exists (many values being even almost identical, see Fig. 6) for the ^{2}H and ^{6}Li abundances for all dependences studied here.
- The values found for the current best value $\eta = 6.14 \times 10^{-10}$ [37] were found to be by and large consistent with those cited in [14], if the same assumptions concerning the a_s-dependence (values indicated by $^{(*)}$ in Table 2) and the temperature independent modification of the rates according to Eqs. (19, 25) are made (extracted from the entries indicated by † in Table 2), see Table 3. Note that in [14] a slightly different value $\eta = 6.19 \times 10^{-10}$ was used.
- More importantly, it was found that accounting for the actual a_s dependence in the calculation of the cross section for the $n + p \to d + \gamma$ reaction and, accordingly for a temperature dependence in the corresponding rate, in fact the linear dependence of the abundances on this scattering length is reduced with respect to the temperature independent a_s^2 dependence assumed in [14] approximately by a factor of three.
- Also, accounting for the temperature dependence in the rate when varying the bindings energies of at least the leading reactions in the nuclear BBN network, reduces the values of the response matrix elements in some cases appreciably: In particular this applies to the abundance-dependence of ^{6}Li in the binding energy of ^{6}Li ($\approx 80 \mapsto \approx 75$) and the abundance-dependences of ^{7}Li+^{7}Be on the binding energy of ^{3}H ($\approx 4 \mapsto \approx 3.5$), on the binding energy of ^{3}He ($\approx 8.25 \mapsto \approx 6.75$) and on the binding energy of ^{7}Be ($\approx 100 \mapsto 87$).
- Furthermore, although the numbers found are roughly consistent, see e.g. the ranges listed in Tables 3 and 4, the four publicly available codes, which do differ in the number of coupled reactions treated in the BBN-network, the treatment of radiative corrections to processes as well as the specific parameterization of the nuclear reaction rates, do lead to slightly different values for the response matrix elements studied here.
  We shall therefore consider these differences, see Table 4, as an estimate of the systematic (in fact model-dependent) deviations for the numbers obtained. This is one of the main results of the present investigation. As can also be seen from Fig. 6 the largest relative deviations are found for the dependence of the ^{7}Li + ^{7}Be abundance on the binding energy of ^{2}H with the programme PArtHEnoPE: 20 %. No obvious explanation for this could be found. Also the dependence of the ^{2}H abundance on the binding energy of ^{4}He with the programme alterBBN deviates from those found with the other codes. Note, however, that here an exceptional non-linear dependence on $B_{^4\mathrm{He}}$ was found; determining the logarithmic derivative only from left-sided finite differences yields an almost vanishing value, in accordance with the

Table 2 BBN response matrix $\partial \log Y_n / \partial \log X_k$ at $\eta = 6.14 \times 10^{-10}$ and $\tau_n = 879.4$ s

X	code	^{2}H	^{3}H+^{3}He	^{4}He	^{6}Li	^{7}Li+^{7}Be
a_s	NUC123	−0.12	0.09	0.00	−0.12	0.97
	PArthENoPE	−0.18	0.06	0.04	−0.17	1.07
	alterBBN	−0.13	0.08	0.00	−0.13	0.99
	PRIMAT	−0.13	0.08	0.00	−0.13	0.99
	NUC123(*)	−0.37	0.18	0.01	−0.36	2.52
	PArthENoPE(*)	−0.41	0.15	0.01	−0.41	2.60
	alterBBN(*)	−0.40	0.15	0.01	−0.39	2.57
	PRIMAT(*)	−0.41	0.16	0.01	−0.40	2.58
	Ref. [14]	−0.39	0.17	0.01	−0.38	2.64
$B_{^2\mathrm{H}}$	NUC123	−2.78	−2.08	0.67	−6.26	8.41
	PArthENoPE	−2.49	−2.27	0.68	−5.93	6.16
	alterBBN	−2.93	−2.09	0.69	−6.38	8.76
	PRIMAT	−2.89	−2.11	0.69	−6.33	8.63
	NUC123(†)	−2.74	−2.08	0.67	−6.41	8.36
	PArthENoPE(†)	−2.45	−2.28	0.68	−6.10	6.11
	alterBBN(†)	−2.89	−2.10	0.68	−6.54	8.71
	PRIMAT(†)	−2.85	−2.12	0.68	−6.49	8.59
	Ref. [14]	−2.91	−2.08	0.67	−6.57	9.44
	Ref. [11]	−2.8	−2.1	0.68	−6.8	8.8
	Ref. [12]	−2.91	−2.1	0.67	−6.58	9.41
$B_{^3\mathrm{H}}$	NUC123	−0.32	−2.22	0.01	−0.31	−3.61
	PArthENoPE	−0.28	−2.14	−0.02	−0.27	−3.49
	alterBBN	−0.26	−2.16	0.00	−0.25	−3.60
	PRIMAT	−0.28	−2.20	0.01	−0.27	−3.58
	NUC123(†)	−0.31	−2.39	0.01	−0.29	−3.93
	PArthENoPE(†)	−0.27	−2.29	0.03	−0.26	−3.80
	alterBBN(†)	−0.25	−2.32	0.01	−0.24	−3.92
	PRIMAT(†)	−0.27	−2.37	0.01	−0.25	−3.90
	Ref. [14]	−0.27	−2.36	0.01	−0.26	−3.84
	Ref. [11]	−0.22	−1.4	0	−0.20	−2.5
$B_{^3\mathrm{He}}$	NUC123	−2.35	3.76	0.01	−5.49	−6.47
	PArthENoPE	−2.37	3.67	0.04	−5.61	−6.57
	alterBBN	−2.42	3.68	0.01	−5.66	−6.72
	PRIMAT	−2.36	3.73	0.01	−5.61	−6.75
	NUC123(†)	−2.44	3.94	0.01	−5.66	−8.13
	PArthENoPE(†)	−2.73	3.76	0.11	−6.16	−8.06
	alterBBN(†)	−2.58	3.91	0.01	−5.91	−8.37
	PRIMAT(†)	−2.46	3.91	0.01	−5.79	−8.41
	Ref. [14]	−2.38	3.85	0.01	−5.72	−8.27
	Ref. [11]	−2.1	3.0	0	−3.1	−9.5
$B_{^4\mathrm{He}}$	NUC123	−0.01	−0.79	−0.00	−66.73	−49.91
	PArthENoPE	−0.02	−0.83	0.00	−66.67	−50.14
	alterBBN	−0.08	−0.85	0.00	−66.72	−50.90
	PRIMAT	−0.02	−0.82	0.00	−66.91	−50.48
	NUC123(†)	−0.01	−0.80	−0.00	−69.49	−57.39
	PArthENoPE(†)	−0.02	−0.84	0.01	−69.53	−57.64
	alterBBN(†)	−0.09	−0.86	0.00	−69.49	−58.43

Table 2 continued

X	code	^{2}H	^{3}H+^{3}He	^{4}He	^{6}Li	^{7}Li+^{7}Be
	PRIMAT$^{(\dagger)}$	−0.02	−0.83	0.00	−69.70	−58.06
	Ref. [14]	−0.03	−0.84	0.00	−69.8	−57.4
	Ref. [11]	−0.01	−0.57	0	−59	−57
$B_{^6\mathrm{Li}}$	NUC123	−0.00	0.00	0.00	75.40	0.00
	PArthENoPE	−0.01	−0.01	0.01	75.34	0.02
	alterBBN	0.00	−0.01	0.00	75.35	0.01
	PRIMAT	−0.00	0.00	0.00	75.65	0.00
	NUC123$^{(\dagger)}$	−0.00	0.00	0.00	78.51	0.00
	PArthENoPE$^{(\dagger)}$	0.02	0.01	−0.01	78.60	−0.02
	alterBBN$^{(\dagger)}$	0.00	−0.00	0.00	78.48	0.00
	PRIMAT$^{(\dagger)}$	−0.00	0.00	0.00	78.81	0.00
	Ref. [14]	0.00	0.00	0.00	78.9	0.00
	Ref. [11]	0	0	0	69	0
$B_{^7\mathrm{Li}}$	NUC123	−0.00	−0.00	−0.00	−0.00	−22.65
	PArthENoPE	−0.02	−0.01	0.02	−0.02	−23.12
	alterBBN	0.01	−0.00	−0.00	0.01	−23.17
	PRIMAT	−0.00	−0.00	0.00	−0.00	−23.39
	NUC123$^{(\dagger)}$	−0.00	−0.00	−0.00	−0.00	−23.54
	PArthENoPE$^{(\dagger)}$	0.01	0.01	−0.01	0.01	−24.09
	alterBBN$^{(\dagger)}$	0.01	0.00	−0.00	0.01	−24.09
	PRIMAT$^{(\dagger)}$	−0.00	0.00	0.00	−0.00	−24.31
	Ref. [14]	0.03	0.01	0.00	0.02	−25.1
	Ref. [11]	0	0	0	0	−6.9
$B_{^7\mathrm{Be}}$	NUC123	−0.00	−0.00	0.00	−0.00	86.58
	PArthENoPE	0.02	0.00	−0.01	0.01	87.31
	alterBBN	0.00	0.00	−0.00	0.00	88.47
	PRIMAT	−0.00	−0.00	−0.00	0.00	88.38
	NUC123$^{(\dagger)}$	−0.00	−0.00	0.00	−0.00	97.43
	PArthENoPE$^{(\dagger)}$	−0.02	−0.01	0.00	−0.03	98.25
	alterBBN$^{(\dagger)}$	0.00	−0.00	−0.00	0.00	99.43
	PRIMAT$^{(\dagger)}$	0.00	−0.00	−0.00	0.00	99.33
	Ref. [14]	0.00	0.00	0.00	0.00	99.1
	Ref. [11]	0	0	0	0	81
τ_n	NUC123	0.41	0.14	0.72	1.36	0.44
	PArthENoPE	0.41	0.14	0.74	1.37	0.45
	alterBBN	0.42	0.14	0.73	1.38	0.43
	PRIMAT	0.42	0.14	0.73	1.38	0.44
	Ref. [14]	0.41	0.14	0.72	1.36	0.43
	Ref. [11]	0.41	0.15	0.73	1.4	0.43

Y_n are the number ratios of the abundances relative to hydrogen; Y_p is conventionally the ^{4}He/H mass ratio. The results obtained with the four BBN codes: NUC123 [18], alterBBN [20], PArthENoPE [23], PRIMAT [4] are given in four subsequent rows for each nuclear parameter. Below that, for comparison also listed are the values obtained in [14] (see Table VII), where $\eta = 6.19 \times 10^{-10}$ was used, obtained in [11] (see Table 1), where $\eta = 6.1 \times 10^{-10}$ and $\tau_n = 885.7$ s were used, as well as the dependence on the deuteron binding energy listed in [12] (method 2 in Table 1), where $\eta = 6.22 \times 10^{-10}$ was used. The entries with $^{(*)}$ are obtained by assuming a a_s^2 dependence of the $n + p \to d + \gamma$ rate, as was done in [14]. The entries with $^{(\dagger)}$ ignore the T-dependence of the rates of the leading reactions, as also done in [14]

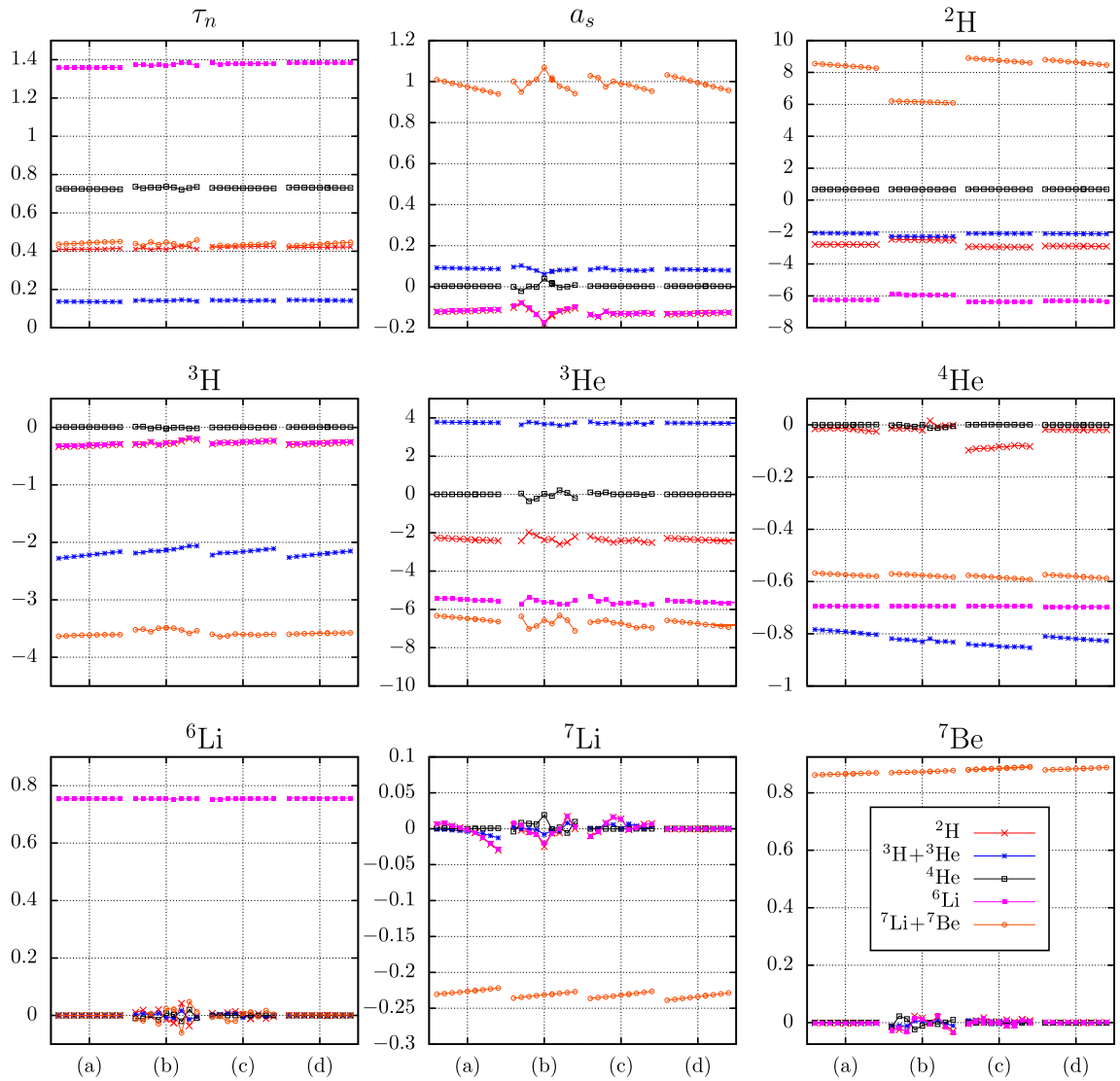

Fig. 6 Baryon-to-photon density η-dependence of the transfer matrix elements $\partial \log Y_n / \partial \log X_k$, $n = {}^2\mathrm{H}$ (crosses in red), ${}^3\mathrm{H} + {}^3\mathrm{He}$ (asterisks in blue), ${}^4\mathrm{He}$ (open squares in black), ${}^6\mathrm{Li}$ (filled squares in magenta) and ${}^7\mathrm{Li} + {}^7\mathrm{Be}$ (open circles in orange; color online). For each of the programmes: **a** `NUC123`, **b** `PArtHEnoPE`, **c** `alterBBN`, **d** `PRIMAT`, the variation of the response matrix elements is shown as 9 subsequent points for $\eta_{10} := \eta \times 10^{10} = 5.94, 5.99, 6.04, 6.09, 6.14, 6.19, 6.24, 6.29, 6.34$, the central values at 6.14 corresponding to the values listed in Table 2. For better visibility, in the panels labeled "^{4}He" and "^{6}Li" the values of the response matrix elements $\partial \log Y_{B_{6_{\mathrm{Li}}}} / \partial \log X_k$ (filled squares, in magenta) have been divided by 100. The same applies to the panels labeled "^{4}He", "^{7}Li" and "^{7}Be" for the response matrix elements $\partial \log Y_{7_{\mathrm{Li}+^7\mathrm{Be}}} / \partial \log X_k$ (open circles, in orange)

values found with the other programmes. The dependence of the ${}^3\mathrm{H} + {}^3\mathrm{He}$ abundance on the binding energy of ^{4}He varies between all programmes by $\approx 8\%$.

5 Summary and conclusion

We reexamined the response matrix elements $\partial \log Y_n / \partial \log X_k$, i.e. the linear fractional change in the abundance Y_n of the nuclides ^{2}H, ${}^3\mathrm{H} + {}^3\mathrm{He}$, ^{4}He, ^{6}Li and ${}^7\mathrm{Li} + {}^7\mathrm{Be}$ due to a fractional change in nuclear parameters X_k: the life time of the neutron τ_n, the ${}^1S_0$ np scattering length a_s and the binding energies of ^{2}H, ^{3}H, ^{3}He, ^{4}He, ^{6}Li, ^{7}Li and ^{7}Be. In addition the dependence of these quantities on the baryon-to-photon density ratio η was studied. In order to obtain an estimate for the model dependence of the response matrix elements, these were determined with four publicly available codes for calculating the abundances of light elements in primordial nucleosynthesis. The calculated values were found to be by and large mutually consistent, the largest deviations were found for matrix elements that almost vanish anyway. Overall systematic deviations between the codes of a few percent do occur, however.

Table 3 Comparison of the range of values obtained with the four codes studied here with the results of [14]

X	^{2}H	^{3}H $+^3$He	Y_p	^{6}Li	^{7}Li $+^7$Be
a_s	−0.41	0.15	0.01	−0.41	2.52
	−0.37	0.18	0.01	−0.36	2.60
	−0.39	0.17	0.01	−0.38	2.64
	−2.89	−2.28	0.67	−6.54	6.11
$B_{^2\mathrm{H}}$	−2.45	−2.08	0.68	−6.10	8.71
	−2.91	−2.08	0.67	−6.57	9.44
	−0.31	−2.39	0.01	−0.29	−3.93
$B_{^3\mathrm{H}}$	−0.25	−2.29	0.03	−0.24	−3.80
	−0.27	−2.36	0.01	−0.26	−3.84
	−2.73	3.76	0.01	−6.16	−8.41
$B_{^3\mathrm{He}}$	−2.44	3.94	0.11	−5.66	−8.06
	−2.38	3.85	0.01	−5.72	−8.27
	−0.09	−0.86	−0.00	− 69.7	−58.4
$B_{^4\mathrm{He}}$	−0.01	−0.80	0.01	−69.5	−57.4
	−0.03	−0.84	0.00	−69.8	−57.4
	−0.00	−0.00	−0.01	78.5	−0.02
$B_{^6\mathrm{Li}}$	0.02	0.01	0.00	78.8	0.00
	0.00	0.00	0.00	78.9	0.00
	−0.00	−0.00	−0.01	−0.00	−24.3
$B_{^7\mathrm{Li}}$	0.01	0.01	0.00	0.01	−23.5
	0.03	0.01	0.00	0.02	−25.1
	−0.02	−0.01	−0.00	−0.03	97.4
$B_{^7\mathrm{Be}}$	0.00	−0.00	0.00	0.00	99.4
	0.00	0.00	0.00	0.00	99.1
	0.41	0.14	0.72	1.36	0.43
τ_n	0.42	0.14	0.74	1.38	0.45
	0.41	0.14	0.72	1.36	0.43

For each parameter X the first two lines then give the minimal and maximal values obtained with the four codes, on the basis of the same assumptions as in [14], i.e. these were extracted from the entries labeled $^{(*)}$ and $^{(\dagger)}$ in Table 2. The third line below the horizontal rule contains the values reported in [14]

Table 4 Model dependence of the response matrix elements

X	^{2}H	^{3}H $+^3$He	Y_p	^{6}Li	^{7}Li $+^7$Be
a_s	−0.18	0.06	0.00	−0.17	0.97
	−0.12	0.09	0.04	−0.12	1.07
$B_{^2\mathrm{H}}$	−2.93	−2.27	0.67	−6.38	6.16
	− 2.49	− 2.07	0.69	− 5.93	8.76
$B_{^3\mathrm{H}}$	− 0.32	−2.22	−0.02	−0.31	−3.61
	−0.26	−2.14	0.01	−0.25	−3.49
$B_{^3\mathrm{He}}$	−2.42	3.67	0.01	−5.66	−6.75
	−2.35	3.76	0.04	−5.49	−6.47
$B_{^4\mathrm{He}}$	−0.08	−0.85	−0.00	−66.9	−50.9
	−0.01	−0.79	0.00	−66.7	−49.9
$B_{^6\mathrm{Li}}$	−0.01	-0.01	0.00	75.3	0.00
	0.00	0.00	0.01	75.7	0.02
$B_{^7\mathrm{Li}}$	−0.02	−0.01	−0.00	−0.02	− 23.4
	0.01	−0.00	0.02	0.01	−22.7
$B_{^7\mathrm{Be}}$	−0.00	−0.00	−0.01	−0.00	86.6
	0.02	0.00	0.00	0.01	88.5
τ_n	0.41	0.14	0.72	1.36	0.43
	0.42	0.14	0.74	1.38	0.45

Listed are the ranges for results extracted from Table 2. For each parameter X the upper row gives the minimal and the lower row the maximal value found with any of the four codes

In the present treatment the nominal values of nuclear binding energies (and hence of nominal Q_0-values) were updated according to the most recent nuclear data bases currently available. Moreover, in contrast to previous studies, we did account for temperature dependences of the sensitivity of the rate of the leading $n + p \rightarrow d + \gamma$ reaction on the $^1S_0$ np scattering length a_s, as well as that of the sensitivity of the rates of a dozen other leading reactions in the BBN-network to the Q-values of these reactions. Both effects lead to a reduction of the magnitude of the response matrix elements: the first effect to a reduction by a factor of three, the latter in some cases approximately by 10% . The η dependence of the response matrix elements was found to be a minor effect only.

These findings should be taken into account before making e.g. claims on bounds from primordial nucleosynthesis on more fundamental parameters, such as quark masses or coupling constants, underlying the nuclear parameters studied here. Here we shall refrain from determining such bounds, postponing that to a future publication and merely mention an important issue to be addressed prior to that. Ideally, a study of varying nuclear parameters in order to investigate their impact on abundances in BBN-nucleosynthesis should rely on accurate theoretical descriptions of at least the major reactions, such that the dependence of the cross sections of the leading reactions on nuclear parameters such as scattering lengths, effective range parameters and binding energies can be determined in detail. Presently such a description is available for the leading $n + p \rightarrow d + \gamma$ reaction only in the form of an accurate EFT-treatment. Therefore this was elaborated on in some detail here. A similar treatment of other reactions is the subject of current research, see e.g. the discussion of $\alpha - \alpha$ scattering in [38]. A first application of the insight obtained here will be a reassessment of the dependence of primordial abundances on the electromagnetic fine-structure constant [39].

Acknowledgements This project is part of the ERC Advanced Grant "EXOTIC" supported the European Research Council (ERC) under the European Union's Horizon 2020 research and innovation programme (Grant agreement no. 101018170), We further acknowledge support by the Deutsche Forschungsgemeinschaft (DFG, German Research Foundation) and the NSFC through the funds provided to the Sino-German Collaborative Research Center TRR110 "Symmetries and the Emer-

gence of Structure in QCD" (DFG Project ID 196253076 - TRR 110, NSFC Grant No. 12070131001), the Chinese Academy of Sciences (CAS) President's International Fellowship Initiative (PIFI) (Grant no. 2018DM0034) and Volkswagen Stiftung (Grant no. 93562).

Funding Information Open Access funding enabled and organized by Projekt DEAL.

Data Availability Statement This manuscript has no associated data or the data will not be deposited. [Authors' comment: All relevant data are given in the tables. Additional data available upon request.]

References

1. K.A. Olive, G. Steigman, T.P. Walker, Phys. Rept. **333**, 389–407 (2000). https://doi.org/10.1016/S0370-1573(00)00031-4. arXiv:astro-ph/9905320 [astro-ph]
2. F. Iocco, G. Mangano, G. Miele, O. Pisanti, P.D. Serpico, Phys. Rept. **472**, 1–76 (2009). https://doi.org/10.1016/j.physrep.2009.02.002. arXiv:0809.0631 [astro-ph]
3. R.H. Cyburt, B.D. Fields, K.A. Olive, T.H. Yeh, Rev. Mod. Phys. **88**, 015004 (2016). https://doi.org/10.1103/RevModPhys.88.015004. arXiv:1505.01076 [astro-ph.CO]
4. C. Pitrou, A. Coc, J.P. Uzan, E. Vangioni, Phys. Rept. **754**, 1–66 (2018). https://doi.org/10.1016/j.physrep.2018.04.005. arXiv:1801.08023 [astro-ph.CO]
5. C.J. Hogan, Rev. Mod. Phys. **72**, 1149–1161 (2000). https://doi.org/10.1103/RevModPhys.72.1149. arXiv:astro-ph/9909295 [astro-ph]
6. J.P. Uzan, Rev. Mod. Phys. **75**, 403 (2003). https://doi.org/10.1103/RevModPhys.75.403. arXiv:hep-ph/0205340 [hep-ph]
7. A.N. Schellekens, Rev. Mod. Phys. **85**(4), 1491–1540 (2013). https://doi.org/10.1103/RevModPhys.85.1491. arXiv:1306.5083 [hep-ph]
8. U.-G. Meißner, Sci. Bull. **60**(1), 43–54 (2015). https://doi.org/10.1007/s11434-014-0670-2. arXiv:1409.2959 [hep-th]
9. J.F. Donoghue, Ann. Rev. Nucl. Part. Sci. **66**, 1–21 (2016). https://doi.org/10.1146/annurev-nucl-102115-044644. arXiv:1601.05136 [hep-ph]
10. F.C. Adams, Phys. Rept. **807**, 1–111 (2019). https://doi.org/10.1016/j.physrep.2019.02.001. arXiv:1902.03928 [astro-ph.CO]
11. T. Dent, S. Stern, C. Wetterich, Phys. Rev. D **76**, 063513 (2007). https://doi.org/10.1103/PhysRevD.76.063513. arXiv:0705.0696 [astro-ph]
12. J.C. Berengut, V.V. Flambaum, V.F. Dmitriev, Phys. Lett. B **683**, 114–118 (2010). https://doi.org/10.1016/j.physletb.2009.12.002. arXiv:0907.2288 [nucl-th]
13. P.F. Bedaque, T. Luu, L. Platter, Phys. Rev. C **83**, 045803 (2011). https://doi.org/10.1103/PhysRevC.83.045803. arXiv:1012.3840 [nucl-th]
14. J.C. Berengut, E. Epelbaum, V.V. Flambaum, C. Hanhart, U.G. Meißner, J. Nebreda, J.R. Pelaez, Phys. Rev. D (2013). https://doi.org/10.1103/PhysRevD.87.085018. arXiv:1301.1738 [nucl-th]
15. D. Lee, U.-G. Meißner, K.A. Olive, M. Shifman, T. Vonk, Phys. Rev. Res. **2**(3), 033392 https://doi.org/10.1103/PhysRevResearch.2.033392. arXiv:2006.12321 [hep-ph]
16. J.W. Chen, M.J. Savage, Phys. Rev. C **60**, 065205 (1999). https://doi.org/10.1103/PhysRevC.60.065205. arXiv:nucl-th/9907042 [nucl-th]
17. G. Rupak, Nucl. Phys. A **678**, 405–423 (2000). https://doi.org/10.1016/S0375-9474(00)00323-7. arXiv:nucl-th/9911018 [nucl-th]
18. L. Kawano, Let's go: Early universe. 2. Primordial nucleosynthesis: The Computer way. Report FERMILAB-PUB-92-004-A (1992)
19. A. Arbey, Comput. Phys. Commun. **183**, 1822–1831 (2012). https://doi.org/10.1016/j.cpc.2012.03.018. arXiv:1106.1363 [astro-ph.CO]
20. A. Arbey, J. Auffinger, K.P. Hickerson, E.S. Jenssen, Comput. Phys. Commun. **248**, 106982 (2020). https://doi.org/10.1016/j.cpc.2019.106982. arXiv:1806.11095 [astro-ph.CO]
21. O. Pisanti, A. Cirillo, S. Esposito, F. Iocco, G. Mangano, G. Miele, P.D. Serpico, Comput. Phys. Commun. **178**, 956–971 (2008). https://doi.org/10.1016/j.cpc.2008.02.015. arXiv:0705.0290 [astro-ph]
22. R. Consiglio, P.F. de Salas, G. Mangano, G. Miele, S. Pastor, O. Pisanti, Comput. Phys. Commun. **233**, 237–242 (2018). https://doi.org/10.1016/j.cpc.2018.06.022. arXiv:1712.04378 [astro-ph.CO]
23. S. Gariazzo, P.F. de Salas, O. Pisanti, R. Consiglio, Comput. Phys. Commun. **271**, 108205 (2022). https://doi.org/10.1016/j.cpc.2021.108205. arXiv:2103.05027 [astro-ph.IM]
24. K.A. Olive, arXiv:2105.04461 [hep-ph]
25. G. Gamow, Z. Physik **51**, 204 (1928)
26. E. Segrè, *Nuclei and Particles*, 2nd edn. (Benjamin, Reading, 1977)
27. NNDC Online Data Service, http://www.nndc.bnl.gov. Accessed 12 Aug 2022
28. H. Arenhövel, M. Sanzone, *Photodosintegration of the Deuteron: A Review of Theory and Experiment* (Springer, Berlin, 1991)
29. H.A. Bethe, C. Longmire, Phys. Rev. **77**, 647–654 (1950). https://doi.org/10.1103/PhysRev.77.647
30. H.A. Bethe, R. Peierls, Proc. R. Soc. A **148**, 146 (1935)
31. M.S. Smith, L.H. Kawano, R.A. Malaney, Astrophys. J. Suppl. **85**, 219–247 (1993). https://doi.org/10.1086/191763
32. P.D. Serpico, S. Esposito, F. Iocco, G. Mangano, G. Miele, O. Pisanti, JCAP **12**, 010 (2004). https://doi.org/10.1088/1475-7516/2004/12/010. arXiv:astro-ph/0408076 [astro-ph]
33. E. Tiesinga, P.J. Mohr, D.B. Newell, B.N. Taylor, Rev. Mod. Phys. **93**, 025010 (2021). https://doi.org/10.1103/RevModPhys.93.025010
34. W.J. Huang, M. Wang, F.G. Kondev, G. Audi, S. Naimi, Chin. Phys. C **45**(3), 030002 (2021). https://doi.org/10.1088/1674-1137/abddb0
35. A. Kramida, Yu. Ralchenko, J. Reader, and NIST ASD Team (2021); NIST Atomic Spectra Database (ver. 5.9), [Online]. National Institute of Standards and Technology, Gaithersburg, MD. https://doi.org/10.18434/T4W30F, https://physics.nist.gov/asd [2022, March 1]
36. P. A. Zyla et al. [Particle Data Group], PTEP **2020**(8), (2020), 083C01 https://doi.org/10.1093/ptep/ptaa104
37. R.L. Workman et al. [Particle Data Group], PTEP **2022**, 083C01 (2022). https://doi.org/10.1093/ptep/ptac097
38. S. Elhatisari, T.A. Lähde, D. Lee, U.-G. Meißner, T. Vonk, JHEP **02**, 1 (2022). https://doi.org/10.1007/JHEP02(2022)001. arXiv:2112.09409 [hep-th]
39. U.-G. Meißner, B. Ch. Metsch , H. Meyer, (**in preparation**)